Photochemistry and Photobiology, 2008, 84: 750–757

Molecular Recognition in Partially Folded States of a Transporter Protein: Temperature-dependent Specificity of Bovine Serum Albumin

Debapriya Banerjee and Samir Kumar Pal*

Unit for Nano Science & Technology, Department of Chemical, Biological & Macromolecular Sciences,
S. N. Bose National Centre for Basic Sciences,
Salt Lake, Kolkata, India

Received 25 July 2007, accepted 18 October 2007, DOI: 10.1111/j.1751-1097.2007.00252.x

ABSTRACT

The specificity of molecular recognition of a transporter protein bovine serum albumin (BSA) in its different partially folded states has been studied. In order to avoid complications due to chemical denaturation, we have prepared thermally induced partially folded states of the protein. The partially folded states have been structurally characterized by circular dichroism and differential thermal analysis techniques. The change in the globular structure of the protein as a consequence of thermal unfolding has also been characterized by dynamic light scattering. Steady state, picosecond-resolved fluorescence and polarization gated spectroscopies on the ligands (DCM, LDS 750) in the protein reveal the dynamics of the binding sites and the specificity of ligand binding of BSA. Picosecond resolved Förster resonance energy transfer studies on the donor DCM and acceptor LDS 750 confirm that the specificity of ligand binding in the binding site is maintained up to 70°C. At 75°C, the protein loses its specificity of recognition at the aforesaid site.

INTRODUCTION

Proteins are like molecular machines, building blocks and arms of a living cell. Enormous variety of protein functions like enzymatic activity and transport of substances are based on the highly specific recognition of the target molecules by the concerned protein. Serum albumins are an important class of transport proteins in mammals (1). These proteins transport a wide variety of substances in the blood stream. These substances or ligands, which are transported by the protein, are often bound noncovalently to the various binding sites of the protein through hydrogen bonds and hydrophobic interactions (2–4). Among the different serum albumins, the structure and properties of the human serum albumin (HSA) and bovine serum albumin (BSA) have been most widely investigated (5–12). The X-ray crystal structure of HSA shows the existence of three helical domains (I–III) in the protein molecule with eight pairs of double disulphide bridges (5,6). Each domain is further divided into two subdomains (A and B). The binding sites of the ligands are located in the hydrophobic pockets in the sub domains IIA and IIIA of the molecule (4–6). There is no binding site in the domain I of the protein (5,6). The structure of BSA is almost entirely similar to that of its human analog, except for an additional tryptophan residue at position 134 in domain I. The binding of the ligands to their respective binding sites in these proteins is highly specific. This specificity requires a definite, stable and rather rigid three-dimensional arrangement of the protein. As the native protein unfolds under the influence of different perturbations like temperature, pressure and chemicals, the three-dimensional structure of proteins is partially or completely lost (10,12) in the unfolded state. The unfolding dynamics of the proteins HSA/BSA has been monitored using calorimetric (11,13–16) and spectroscopic techniques (8,17,18). The Differential Scanning Calorimetric studies on the aforesaid transport proteins under different conditions of pH and ionic strength suggest that the unfolding of the protein takes place with the formation of a definite intermediate (14,15). Circular dichroism (CD) (10) and vibrational CD (12) studies on BSA at different temperatures show that the alpha helicity of the protein decreases from 66% in the native state at room temperature to 44% at 65°C indicating some loss in secondary structure in the temperature-induced denaturation of the protein (10,12,19). Spectroscopic studies on a fluorescent probe acrylodan covalently attached to the cysteine residue (Cys35) present in domain I of the protein HSA coupled with that on the tryptophan residue (Trp214) present in domain II of the protein HSA under guanidine induced denaturation of the protein suggest that domain II unfolds first followed by the unfolding of domain I (8). The report (8) also suggests that the thermal-denaturation of the protein follows a similar pathway. Solvation dynamics of the above mentioned probes in the chemically denatured HSA have also been studied in a separate report (17).

The spectroscopic probes in all these studies (8,17) are covalently bound ligands, which are unlikely to leave the protein as it unfolds under the experimental conditions. These covalently bound ligands can successfully report the dynamics of the unfolded protein, however, they cannot give any information about the molecular recognition of ligands, which as mentioned above are generally noncovalently but specifically bound to the protein in the native state. A survey of the existing literature shows that although the thermal unfolding process of the protein has been studied in much detail, the molecular recognition of the protein in the

*Corresponding author email: skpal@bose.res.in (Samir Kumar Pal)

partially folded states has not yet been addressed. The investigation of the specificity of molecular recognition in the partially folded states of the protein is important to get an insight into the robustness of the process of molecular recognition. In the case of the transport protein BSA, which can transport a wide variety of drug molecules, the knowledge of the recognition process in partially folded states can be of potential use in pharmacy for the design of new drugs. Another important application of the molecular recognition is in the synthesis of nanomaterials *via* biomimetic route using the transporter protein molecule as a template (20,21).

In our present communication, we have studied the specificity of molecular recognition in the different unfolded states of BSA by monitoring the competitive binding between two ligands 2-[4-[4-(dimethylamino)phenyl]-1,3-butadienyl]-3-ethyl-naphtho[2,1-d]thiazolium perchlorate (LDS 750) and 4-dicyanomethylene-2-methyl-6-(*p*(dimethylamino)styryl)-4H-pyran (DCM). Both the probes show fluorescence enhancement and blueshift upon complexation with the protein at room temperatures indicating that the probes are bound to the hydrophobic pockets in the binding sites of BSA. We have studied the temperature-induced denaturation of the protein to avoid complicacies of competitive binding in chemical-induced denaturation. Picosecond-resolved polarization gated anisotropies have been used to study the geometrical restrictions and hence the binding of the protein in the partially folded states at different temperatures. Forster's resonance energy transfer (FRET) has been used to estimate the distance between the two probe molecules attached simultaneously in the different binding sites of the protein. The partially folded states of the protein have been characterized from their secondary and globular structures determined by CD and dynamic light scattering (DLS) studies. The energy profile for the different unfolded states has been constructed using the differential thermal analysis (DTA) and temperature dependent CD/UV absorption studies of the protein in buffer. The steady state and FRET studies on the ligand-bound BSA reveal the nature of specific recognition of the binding site in the protein, which is lacking in the recent literature.

MATERIALS AND METHODS

BSA and phosphate buffer are obtained from Sigma. The purity of the protein has been checked by gel electrophoresis and found to be 99% pure and essentially free from fatty acids and globulin. The fluorescent probes LDS 750 and DCM are from Exciton. Cetyltrimethylammonium bromide (CTAB) is from Fluka. The sample solutions are prepared in 50 mM phosphate buffer using water from Millipore system. The probe-protein solutions are prepared by injecting concentrated ethanolic probe solutions into the aqueous protein solutions and mixing by continuous stirring for 1 h. The probe-protein mixtures are dialyzed against phosphate buffer to avoid free probes in the solution. To ensure complete complexation of the probes with the protein, the [probe]:[protein] ratio is maintained at 1:50 for all the probes in the fluorescence studies. For FRET studies the concentration of the acceptor (LDS 750) is much greater than that of the donor (DCM) and is comparable to that of the protein. The DLS and the DTA studies are carried out using 100 μM BSA solution. The CD studies are done in 1 μM protein solution in 1 cm path-length cell.

Temperature-dependent steady state absorption and emission are measured with Shimadzu Model UV-2450 spectrophotometer and Jobin Yvon Fluoromax-3 fluorimeter, respectively, with a temperature controller attachment from Julabo (Model: F32). DLS measurements are done with Nano S Malvern-instruments employing a 4 mW He–Ne laser (λ = 632.8 nm) and equipped with a thermostatted sample chamber. All the scattered photons are collected at 173° scattering angle at 298 K. The scattering intensity data are processed using the instrumental software to obtain the hydrodynamic diameter (dH) and the size distribution of the scatterer in each sample. The instrument measures the time-dependent fluctuation in the intensity of light scattered from the particles in solution at a fixed scattering angle. Hydrodynamic diameters (dH) of the particles are estimated from the intensity auto-correlation function of the time-dependent fluctuation in intensity. dH is defined as,

$$\mathrm{dH} = k\mathrm{T}/3\pi\eta D, \tag{1}$$

where k = Boltzmann constant, T = absolute temperature, η = viscosity coefficient of the solvent and D = translational diffusion coefficient. In a typical size distribution graph from the DLS measurement, X-axis shows a distribution of size classes in nm, while the Y-axis shows the relative intensity of the scattered light. This is therefore known as an intensity distribution graph. The DTA is done in a Diamond TG/DTA instrument from Perkin Elmer. The CD measurements are done in a JASCO 815 spectrometer with an attachment for the temperature dependent measurements (Peltier). The secondary structural data of the CD spectra are analyzed using CDNN software.

Fluorescence transients are measured and have been fitted by using a commercially available spectrophotometer (LifeSpec-ps) from Edinburgh Instrument, UK (excitation wavelengths 409 nm [for DCM] and 633 nm [for LDS 750], 80 ps instrument response function) with an attachment for temperature-dependent studies. The observed fluorescence transients are fitted by using a nonlinear least square fitting procedure to a function ($X(t) = \int_0^t E(t')R(t-t')dt'$) comprising of convolution of the IRF (E(t)) with a sum of exponentials ($R(t) = A + \sum_{i=1}^{N} B_i e^{-t/\tau_i}$) with pre-exponential factors (B_i), characteristic lifetimes (τ_i) and a background (A). Relative percentage in a multi-exponential decay is finally expressed as $c_n = \mathrm{B}_n/\sum_{i=1}^{N} B_i \times 100$. The quality of the curve fitting is evaluated by reduced chi-squared and residual data. For anisotropy (r[t]) measurements, emission polarization is adjusted to be parallel or perpendicular to that of the excitation and anisotropy is defined as $r(t) = [I_{\mathrm{para}} - G \times I_{\mathrm{perp}}]/[I_{\mathrm{para}} + 2 \times G \times I_{\mathrm{perp}}]$. G, the grating factor is determined following longtime tail matching technique (22) to be 1.2. In order to estimate the fluorescence resonance energy transfer efficiency of the donor (DCM) to the acceptor (LDS 750) and hence to determine distances of donor–acceptor pairs, we followed the methodology described in chapter 13 of reference (23). The Förster distance (R_0) is given by,

$$\mathrm{R}_0 = 0.211[\kappa^2 \mathrm{n}^{-4} Q_{\mathrm{D}} \mathrm{J}(\lambda)]^{1/6} \quad (\text{in Å}) \tag{2}$$

where κ^2 is a factor describing the relative orientation in space of the transition dipoles of the donor and acceptor. For donor and acceptors that randomize by rotational diffusion prior to energy transfer, the magnitude of κ^2 is assumed to be 2/3. In the present study, the same assumption has been made. The refractive index (n) of the medium is assumed to be 1.4. Q_{D}, the quantum yield of the donor in the absence of acceptor is measured to be 0.42 and 0.45 in protein and CTAB micelles, respectively. J(λ), the overlap integral, which expresses the degree of spectral overlap between the donor emission and the acceptor absorption, is given by,

$$\mathrm{J}(\lambda) = \frac{\int_0^\infty F_{\mathrm{D}}(\lambda)\varepsilon(\lambda)\lambda^4 d\lambda}{\int_0^\infty F_{\mathrm{D}}(\lambda) d\lambda} \tag{3}$$

where $F_{\mathrm{D}}(\lambda)$ is the fluorescence intensity of the donor in the wavelength range of λ to λ + dλ and is dimensionless. $\varepsilon(\lambda)$ is the extinction coefficient (in M^{-1} cm^{-1}) of the acceptor at λ. If λ is in nm, then J(λ) is in units of M^{-1} cm^{-1} nm^4. Once the value of R_{o} is known, the donor–acceptor distance (r) can easily be calculated using the formula,

$$r^6 = [R_0^6(1-E)]/E \quad (4)$$

Here E is the efficiency of energy transfer. The efficiency E is calculated from the lifetimes under these respective conditions (τ_D and τ_{DA}).

$$E = 1 - (\tau_{DA}/\tau_D) \quad (5)$$

RESULTS AND DISCUSSION

The unfolding of a protein is marked by a change in the secondary and globular structure of the protein. Figure 1a and b shows the change in the hydrodynamic radius and the percentage helicity of the protein, respectively, at various temperatures. Both the curves show changes in slopes indicating the presence of intermediates in the melting profile of the protein. It is to be noted that the presence of intermediate unfolded states in the thermal and chemical denaturation of BSA has already been indicated by calorimetric (15) and spectroscopic (8,17) studies. Careful inspection of the curves in Fig. 1a and b reveal that there are three unfolded states at three consecutive temperatures around 50°C, 64°C and 75°C, respectively. To obtain a more quantitative picture of the unfolding process and to construct an energy profile of the unfolding of the protein, DTA studies are carried out on the protein in buffer. Figure 2 shows the DTA pattern of 100 μM of the protein in buffer. Arrows show the onsets of the changes in slope of the thermogram. The total endothermic area under the curve could be resolved into three separate curves (deconvolution) having peaks around 54°C, 64°C and 72°C (Fig. 2b), indicating three transitions take place in the protein around these three temperatures. It is to be noted that the transition temperatures obtained from the DTA measurements tally quite well with that obtained from the DLS and CD results (Fig. 1a and b). The peak coming in the exothermic region at temperatures around 80°C is associated with thermal aggregation of the protein at the higher temperature (24). The area under each deconvoluted curve gives the heat energy change (ΔH) associated with the corresponding structural transition. The ΔH values associated with the transitions have been tabulated in Table 1. The observed ΔH values are in good accordance with previously reported result (15). The free energy change (ΔG) associated with the transitions has been estimated from the relation (24,25),

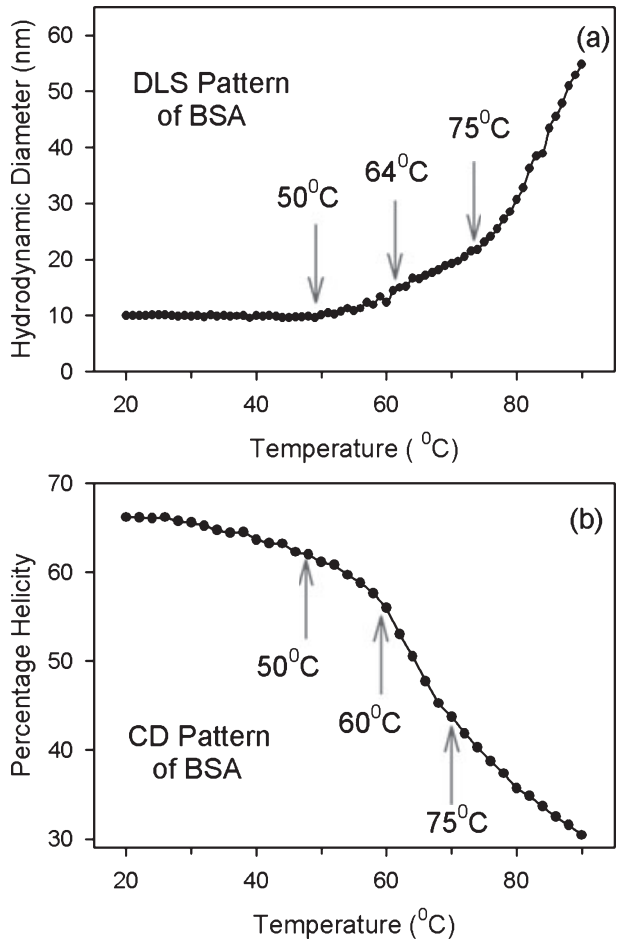

Figure 1. The hydrodynamic diameter (a) and the percentage helicity (b) of 100 μM BSA in phosphate buffer. The arrows indicate the change in slope of the curve reflecting the structural transitions of the protein. (b) The deconvoluted DTA profile of BSA in phosphate buffer.

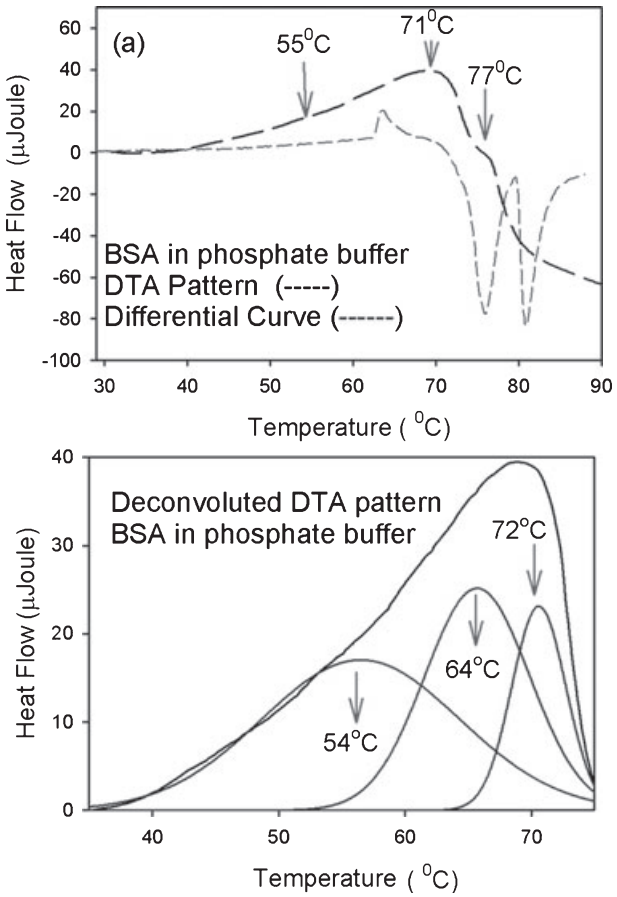

Figure 2. The DTA pattern of 100 μM BSA in phosphate buffer. The arrows indicate the change in slope of the curve reflecting the structural transitions of the protein.

Table 1. Thermodynamic parameters associated with temperature-induced denaturation of BSA.

Parameter	Transition 1 (Native → Intermediate 1)	Transition 2 (Intermediate 1 → Intermediate 2)	Transition 3 (Intermediate 2 → Unfolded)
Temperature (°C)	50	64	75
ΔH (KJ mol^{-1})	212	210	230
ΔG (KJ mol^{-1}) (from extinction coefficient)	2.314	2.279	–
ΔG (KJ mol^{-1}) (from CD)	1.797	1.951	–

CD, circular dichroism; BSA, bovine serum albumin.

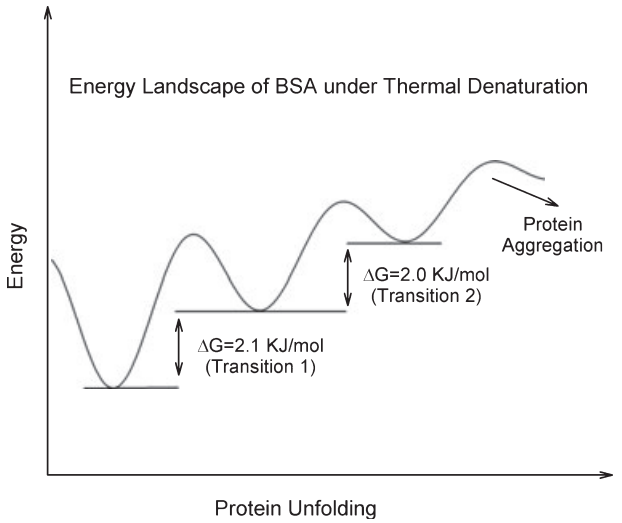

Scheme 1. The free energy landscape (not drawn to scale) of the protein BSA under thermal denaturation.

$$\Delta G = -RT \ln K \tag{11}$$

where K is the equilibrium constant associated with the transition,

$$N \leftrightarrow D \tag{12}$$

where N denotes the native and D is the denatured or partly denatured state and is given by the relation,

$$K = [\text{native}]/[\text{denatured}] \tag{13}$$

The ratio of the concentrations of the native and denatured states could be obtained from the relation,

$$K = (P_{eq} - P_n)/(P_d - P_{eq}) \tag{14}$$

where P is any property, which changes from the native (P_n) to the denatured (P_d) state. P_{eq} is the corresponding value at equilibrium. These properties in the case of proteins are the extinction coefficient, the secondary or globular structure, and other properties (24). In the present study the ΔG values have been independently calculated for the reversible transitions monitoring independently the changes in extinction coefficient and the percentage of helicity (secondary structure) values at different temperatures and the values are found to be consistent. The average ΔG values associated with the transitions are tabulated in Table 1. The free energy landscape of the protein BSA under thermal denaturation is shown in Scheme 1. Our observations suggest that there are intermediate states associated with the thermal unfolding of BSA.

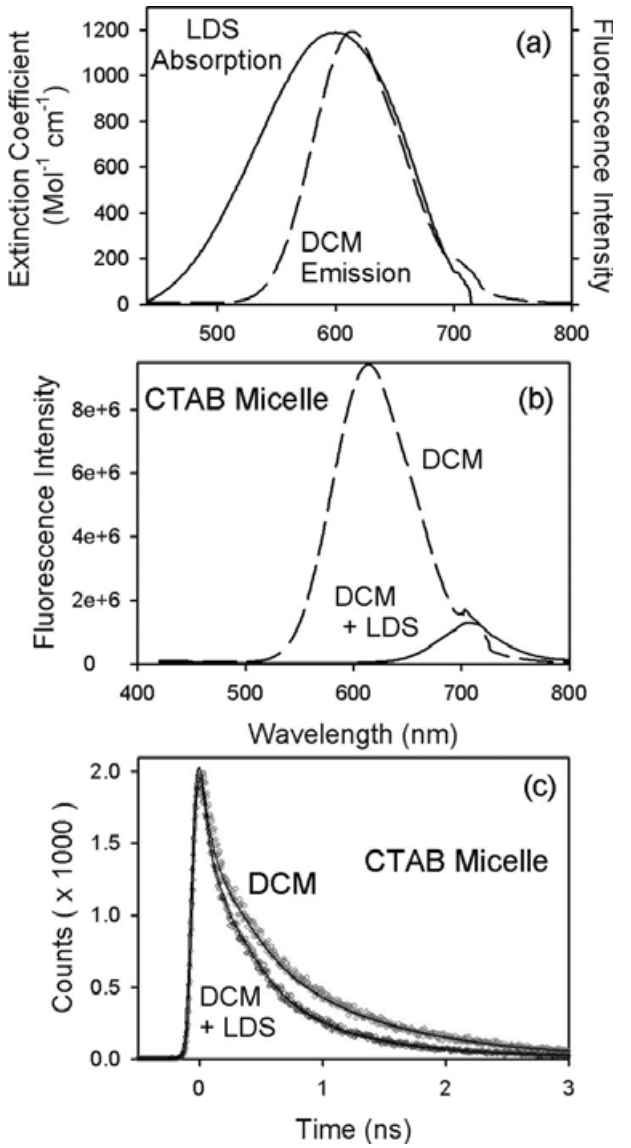

Figure 3. (a) The absorption spectrum of LDS 750 and the emission spectra of DCM in CTAB micelles. The emission spectra (b) and fluorescence transients (c) of DCM and DCM-LDS 750 in CTAB micelles.

The picosecond-resolved solvation studies on BSA with LDS 750 and DCM at various temperatures (see Supplementary

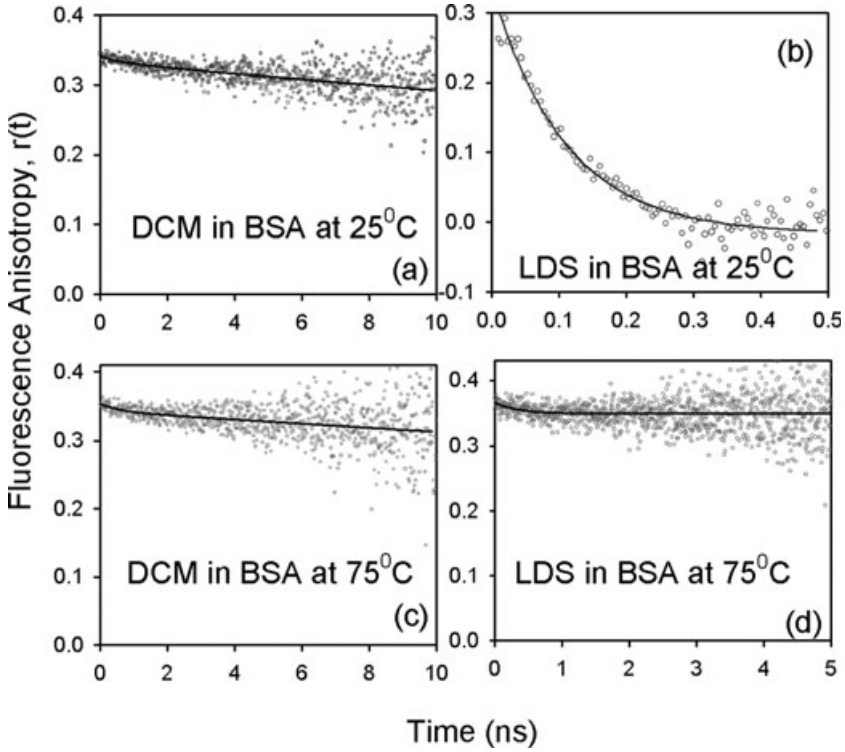

Figure 4. The temporal decay of fluorescence anisotropies, r(t) of DCM [[DCM] = 1 μM] and LDS 750[[LDS 750] = 100 μM] in BSA solution containing both the probes at different temperatures.

materials) show the similarity of the binding nature of LDS 750 and DCM, indicating a possibility of binding of the ligands to similar sites in the protein. DCM is extremely hydrophobic and completely insoluble in water. In the protein it occupies the binding site for hydrophobic residues and therefore, a possible location of the probe is at the binding site in domain IIIA (5). On the other hand LDS 750 is a cationic dye with a large hydrophobic moiety. Early studies (26,27) of the binding of cationic surfactants with a hydrophobic alkyl chain explored the possible locations of the surfactants are Sudlow I and Sudlow II regions (27) which are close to subdomains IIA and IIIA, respectively. The binding affinity of LDS 750 to Sudlow II regions (subdomain IIIA) might direct the ligand to subdomain IIIA, which is also the possible binding site of DCM (5). Addition of excess LDS 750 to the solution of DCM–BSA complex shows a significant redshift of 10 nm (data not shown) in the emission of DCM, reflecting the expulsion of DCM from BSA as a consequence of competitive binding with LDS 750. The observation indicates specific recognition of the ligand at a particular site (possibly the Sudlow region II or equivalent site II in subdomain IIIA) of BSA, when one ligand occupies the site the other ligand cannot be recognized by the protein. In order to explore the further possibility of binding of the two ligands simultaneously in the protein, we have used FRET techniques. The significant spectral overlap of DCM emission with the absorption of LDS 750 is expected to reveal inter-ligand distance, when they are in close proximity. To check the possibility of FRET between DCM and LDS 750, we study CTAB micelles where both the ligands bind at the micellar surface. Figure 3a shows the normalized DCM (donor) emission and LDS 750 (acceptor) absorption in CTAB micelles at room temperature. Figure 3b shows the emission of the donor and that of the donor acceptor complex. The figure shows that the emission from the donor gets quenched due to absorption by the acceptor. This quenching of the donor emission is further evident from the faster lifetime associated with the donor–acceptor (DCM-LDS 750) complex compared with that in donor (DCM) only in CTAB micelles (Fig. 3c). The Forster distance, R_0 for the donor and the donor–acceptor complex is calculated to be 2.8 nm. The distance between the probes is 2.4 nm. This distance corresponds to the length of the chord separating the DCM and the LDS 750 molecules, both of which are located at the surface of the micelle with dH of 12 nm (28).

The R_0 value for the probes DCM and LDS 750 in the protein solution at room temperature has been calculated to be 3.26 nm. The inter-domain distance in the protein has been estimated to be 3.18 nm (domain I and II), 2.58 nm (domain II and III) and 2.50 nm (domain I and III) (29). Thus it is obvious that FRET is expected to reveal the inter-ligand distance if they are simultaneously bound to BSA. However, DCM in BSA solution in the presence of LDS 750 at room temperature (25°C) does not show quenching of donor fluorescence in either steady state or temporal decay of the donor molecules in the donor–acceptor complexes. The binding of DCM to the BSA solution containing both the probes (DCM and LDS) at room temperature has been borne out by the presence of a 50 ns component associated with the temporal decay of fluorescence anisotropy (Fig. 4a), indicating the global motion of the protein. The absence of

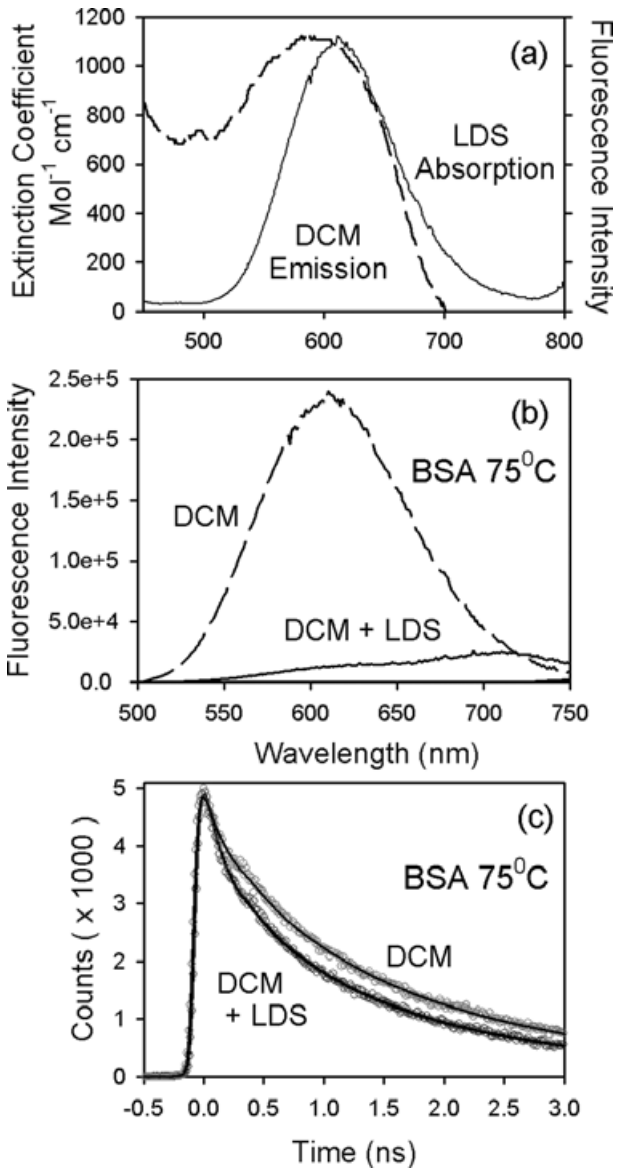

Figure 5. (a) The absorption spectrum of LDS 750 and the emission spectra of DCM in BSA at 75°C. The emission spectra (b) and fluorescence transients (c) of DCM and DCM-LDS 750 in BSA at 75°C.

longer components in the temporal decay of the fluorescence anisotropy of the probe LDS 750 in the DCM–BSA complex (Fig. 4b) show that the probe is not bound to the protein at room temperature. This clearly indicates that simultaneous binding and hence energy transfer does not take place between the probes in the protein solution at room temperature. This confirms that the probes DCM and LDS 750 do not bind to the different domains in the protein. In other words the probes DCM and LDS 750 compete for the same binding site in the protein. To study the effect of temperature on the specificity of binding, or in other words, to study the specificity of ligand binding in the different unfolded states associated with the temperature-induced denaturation of the protein, the energy transfer experiments are carried out at the different temperatures. The binding of the DCM to the protein at different temperatures is borne out by the long component in the temporal decay of the fluorescence anisotropy at different temperature. It is observed that the energy transfer between the donor (DCM) and acceptor (LDS 750) does not take place at intermediate temperatures of 50°C, 60°C or 70°C (data not shown), showing that the specificity of LDS 750 binding is retained even when the structural integrity of the protein is substantially lost (as indicated in the DLS and CD profile). The observation indicates that even at 70°C, the protein is not completely unfolded reflecting the existence of a transition temperature greater than 70°C. A transition temperature greater than 70°C is evidenced from three-intermediates fitting of the DLS, CD and DTA profiles. The energy transfer between the probes DCM and LDS 750 finally takes place at 75°C. The binding of both the ligands at the high temperature is indicated by a long component in the temporal decay of the fluorescence anisotropies (Fig. 4c and d). Figure 5a shows the normalized DCM (donor) emission and LDS 750 (acceptor) absorption in BSA at 75°C. Figure 5b shows the quenching of the DCM (donor) emission in the DCM–protein and the DCM–LDS 750-protein complex at 75°C. The quenching of the donor fluorescence at 75°C is also reflected in the decrease in the lifetime of the donor in the DCM–LDS 750–protein complex as shown in Fig. 5c. The average lifetime of the donor in the protein at 75°C is 1.28 ns whereas that of the donor in the presence of acceptor is 0.882 ns. The R_0 distance associated with the energy transfer at this elevated temperature is 2.98 nm and the distance between the probes is 2.8 nm. The possibility of binding of LDS 750 to a protein aggregate (dH = 25 nm) at 75°C can be ruled out by the following control experiment. It is observed from DLS measurements that the dH of 25 nm does not return to that of the native protein (10 nm) upon cooling to room temperature. The observation is consistent with the results obtained from another study on the thermal unfolding of the protein HSA (8). The swelled protein (dH = 25 nm) at room temperature is found to be unable to bind LDS 750. If the swelled protein is a protein aggregate, then it should be able to bind LDS 750. The lack of intramolecular energy transfer between DCM molecules in the swelled protein at room temperatures also stands against the aggregation at elevated temperature. The results clearly indicate that LDS 750 binds to a nonspecific site in the presence of DCM in the unfolded BSA at 75°C. This shows that the molecules DCM and LDS 750 are simultaneously binding to the BSA and that the binding has lost its specific nature. In other words the binding of ligands to BSA loses its specificity only when the protein is denatured.

CONCLUSION

In the present study, we have explored for the first time the specificity of molecular recognition of a transporter protein BSA in its various partially folded states. We have prepared the partially folded states by using thermal denaturation to avoid the complications due to chemical denaturation. The thermal denaturation of BSA in phosphate buffer at pH 7.0 shows that three intermediate unfolded states are associated with the thermal unfolding. A comparison of the changes in

the secondary (CD) and globular tertiary (DLS) structure of the protein with the DTA studies suggests that the structural transitions take place around 50°C, 64°C and 75°C, respectively. It is observed that the recognition by DCM and LDS 750 is very specific at their particular binding site in BSA. Competitive binding studies on DCM and LDS 750 to BSA and FRET reveal very specific nature of recognition of the protein; when one ligand is bound to BSA, the other cannot get entry to the protein over a wide range of temperature. However, at higher temperatures the two ligands can be bound simultaneously, reflecting nonspecific nature of recognition of BSA. Our studies show that the binding of ligands to BSA is specific, and the specificity is destroyed in the unfolded state of the protein.

Acknowledgements—D.B. thanks CSIR for fellowship. We thank DST for financial grant (SR/FTP/PS-05/2004).

SUPPLEMENTAL MATERIALS

The following supplemental materials are available for this article:

Figure S1. (a) The fluorescence transients in the blue and red end of the probe LDS 750 in BSA at 25°C. We have acquired 15 such transients to construct time-resolved emission spectra (TRES). (b) The TRES of the probe LDS 750 in BSA at 25°C.

Figure S2. The temporal decay of solvation correlation function, C(t) and fluorescence anisotropy, r(t) (inset) of the probe LDS 750 in BSA at 25°C.

Figure S3. (a) The temporal decays of the solvation correlation function C(t) of the probe LDS 750 in BSA at 50°C and 75°C. The decay of fluorescence anisotropies, r(t) of the probe LDS 750 in BSA at 50°C (b) and 75°C (c).

Figure S4. The temporal decays of the solvation correlation function, C(t) of the probe DCM in BSA at different temperature.

Figure S5. The temporal decays of fluorescence anisotropies r(t) of the probe DCM in BSA at temperatures 25°C (a), 50°C (b) and 75°C (c).

Figure S6. The temporal decays of the solvation correlation function C(t) of the probe Coumarin 500 in BSA at different temperature.

Figure S7. The temporal decays of fluorescence anisotropies r(t) of the probe Coumarin 500 in BSA at temperatures 25°C (a), 50°C (b) and 75°C (c).

Table S1. Solvation correlation function at different temperatures.

Table S2. Fluorescence anisotropy at different temperatures.

Detailed instrumental techniques, solvation studies of partially folded states of BSA are provided in this section.

This material is available as part of the online article from: http://www.blackwell-synergy.com/doi/full/10.1111/j.1751-1097.2007.00252.x.

Please note: Blackwell Publishing are not responsible for the content or functionality of any supplementary materials supplied by the authors. Any queries (other than missing material) should be directed to the corresponding author for the article.

REFERENCES

1. de Wolf, F. A. and G. M. Brett (2000) Ligand binding proteins: Their potential for application in systems for controlled delivery and uptake of ligands. *Pharmacol. Rev.* **52**, 207–236.
2. Watanabe, H., S. Tanase, K. Nakajou, T. Maruyama, U. Kragh-Hansen and M. Otagiri (2000) Role of Arg-410 and Tyr-411 in human serum albumin for ligand binding and esterase-like activity. *Biochem. J.* **349**, 813–819.
3. Peyrin, E., Y. C. Guillaume and C. Guinchard (1999) Characterization of solute binding at human serum albumin site II and its geometry using a biochromatographic approach. *Biophys. J.* **77**, 1206–1212.
4. Sudlow, G., D. J. Birkett and D. N. Wade (1975) The characterization of two specific drug binding sites on human serum albumin. *Mol. Pharmacol.* **11**, 824–832.
5. He, X. M. and D. C. Carter (1992) Atomic structure and chemistry of human serum albumin. *Nature* **358**, 209–215.
6. Sugio, S., A. Kashima, S. Mochizuki, M. Noda and K. Kobayashi (1999) Crystal structure of human serum albumin at 2.5 Å resolution. *Prot. Eng.* **12**, 439–446.
7. Qiu, W., L. Zhang, Y. Yang, O. Okobiah, L. Wang, D. Zhong and A. H. Zewail (2006) Ultrafast solvation dynamics of human serum albumin: Correlations with conformational transitions and site selected recognition. *J. Phys. Chem. B* **110**, 10540–10549.
8. Flora, K., J. D. Brennan, G. A. Baker, M. A. Doody and F. V. Bright (1998) Unfolding of acrylodan-labeled human serum albumin probed by steady-state and time-resolved fluorescence methods. *Biophys. J.* **75**, 1084–1096.
9. Takeda, K. and Y. Moriyama (1997) The interaction of bovine serum albumin with sodium dodecyl sulfate: Binding of the surfactant and conformational change of the protein induced by the binding. *Curr. Topics Coll. Intf. Sc.* **1**, 109–135.
10. Takeda, K., A. Wada, K. Yamamoto, Y. Moriyama and K. Aoki (1989) Conformational change of bovine serum albumin by heat treatment. *J. Prot. Chem.* **8**, 653–659.
11. Kosa, T., T. Maruyama and M. Otagiri (1998) Species differences of serum albumins: II. Chemical and thermal stability. *Pharma. Res.* **15**, 449–454.
12. Shanmugam, G. and P. L. Polavarapu (2004) Vibrational circular dichroism spectra of protein films: Thermal denaturation of bovine serum albumin. *Biophys. Chem.* **111**, 73–77.
13. Yamasaki, M., T. Yamashita, H. Yano, K. Tatsumi and K. Aoki (1996) Differential scanning calorimetric studies on bovine serum albumin IV. Effect of anionic surfactants with various lengths of hydrocarbon chain. *Int. J. Biol. Macromol.* **19**, 241–246.
14. Yamasaki, M., H. Yano and K. Aoki (1990) Differential scanning calorimetric studies on bovine serum albumin: I. Effects of pH and ionic strength. *Int. J. Biol. Macromol.* **12**, 263–268.
15. Giancola, C., C. de Sena, D. Fessas, G. Graziano and G. Barone (1997) DSC studies on bovine serum albumin denaturation effects of ionic strength and SDS concentration. *Int. J. Biol. Macromol.* **20**, 193–204.
16. Brandes, N., P. B. Welzel, C. Werner and L. W. Kroh (2006) Adsorption-induced conformational changes of proteins onto ceramic particles: Differential scanning calorimetry and FTIR analysis. *J. Coll. Int. Sci.* **299**, 56–69.
17. Kamal, J. K. A., L. Zhao and A. H. Zewail (2004) Ultrafast hydration dynamics in protein unfolding: Human serum albumin. *Proc. Natl Acad. Sci. USA* **101**, 13411–13416.
18. Takeda, K. and K. Yamamoto (1989) Fluorescence lifetime and rotational correlation time of bovine serum albumin–sodium dodecyl sulphate complex labeled with 1-dimethylaminonaphthalene-5-sulphonyl chloride: Effect of disulphide bridges in the protein on the fluorescence parameters. *J. Prot. Chem.* **9**, 17–22.
19. Moriyama, Y., Y. Kawasaka and K. Takeda (2003) Protective effect of small amounts of sodium dodecyl sulphate on the helical structure of bovine serum albumin in thermal denaturation. *J. Coll. Int. Sci.* **257**, 41–46.
20. Lindman, S., I. Lynch, E. Thulin, H. Nilsson, K. A. Dawson and S. Linse (2007) Systematic investigation of the thermodynamics of HSA adsorption to N-iso-propylacrylamide/N-tert-butylacrylamide copolymer nanoparticles. Effects of particle size and hydrophobicity. *Nano. Lett.* **7**, 914–920.

21. Azioune, A., A. B. Slimane, L. A. Hamou, A. Pleuvy, M. M. Chehimi, C. Perruchot and S. P. Armes (2004) Synthesis and characterization of active ester-functionalized polypyrrole-silica nanoparticles: Application to the covalent attachment of proteins. *Langmuir* **20**, 3350–3356.
22. O'Connor, D. V. and D. Philips (1984) *Time Correlated Single Photon Counting*. Academic Press, London.
23. Lakowicz, J. R. (1999) *Principles of Fluorescence Spectroscopy*. Kluwer Academic/Plenum, New York.
24. Cooper, A. (1999) Thermodynamics of protein folding and stability. *Protein: A Comprehensive Treatise* **2**, 217–270.
25. Brandts, J. F. (1964) The thermodynamics of protein denaturation. I. The denaturation of chymotrypsinogen. *J. Am. Chem. Soc*. **86**, 4291–4301.
26. Peyre, V., V. Lair, V. Andre, G. le Maire, U. Kragh-Hansen, M. le Maire and J. V. Moller (2005) Detergent binding as a sensor of hydrophobicity and polar interactions in the binding cavities of proteins. *Langmuir* **21**, 8865–8875.
27. Peters, T. J. (1996) *All About Albumin: Biochemistry, Genetics and Medical Applications*. Academic Press, San Diego, CA.
28. Berr, S. S., E. Caponetti, J. S. Johnson, J. R. R. M. Jones and L. J. Magid (1986) Small-angle neutron scattering from hexadecyltrimethylammonium bromide micelles in aqueous solutions. *J. Phys. Chem*. **90**, 5766–5770.
29. Hagag, N., E. R. Birnbaum and D. W. Darnall (1983) Resonance energy transfer between cysteine-34, tryptophan-214 and tyrosine 411 of human serum albumin. *Biochemistry* **22**, 2420–2427.

Supplementary Information:

Molecular Recognition in Partially Folded States of a Transporter Protein: Temperature-Dependent Specificity of Bovine Serum Albumin

Debapriya Banerjee and Samir Kumar Pal*

Unit for Nano Science & Technology,
Department of Chemical, Biological & Macromolecular Sciences,
S. N. Bose National Centre for Basic Sciences,
Block JD, Sector III, Salt Lake,
Kolkata 700 098, India

*Corresponding Author. Email: skpal@bose.res.in; Fax: 91 33 2335 3477.

Time Resolved Solvation and fluorescence anisotropy Studies at different temperatures.

Methods To construct time-resolved emission spectra (TRES) we follow the technique described in references[1, 2]. As described above the emission intensity decays are analyzed in terms of the multi-exponential model,

$$I(\lambda, t) = \sum_{i=1}^{N} \alpha_i(\lambda) \exp[-t / \tau_i(\lambda)] \ldots\ldots\ldots (1)$$

where $\alpha_i(\lambda)$ are the pre-exponential factors, with $\Sigma\alpha_i(\lambda)=1.0$. In this analysis, we compute a new set of intensity decays, which are normalized so that the time-integrated intensity at each wavelength is equal to the steady-state intensity at that wavelength. Considering $F(\lambda)$ to be the steady-state emission spectrum, we calculate a set of $H(\lambda)$ values using,

$$H(\lambda) = \frac{F(\lambda)}{\int_0^\infty I(\lambda, t)dt} \ldots\ldots\ldots\ldots (2)$$

which for multi-exponential analysis becomes,

$$H(\lambda) = \frac{F(\lambda)}{\sum_i \alpha_i(\lambda)\tau_i(\lambda)} \ldots\ldots\ldots\ldots (3)$$

Then, the appropriately normalized intensity decay functions are given by,

$$I'(\lambda, t) = H(\lambda)I(\lambda, t) = \sum_{i=1}^{N} \alpha'_i(\lambda) \exp[-t / \tau_i(\lambda)] \ldots\ldots (4)$$

where $\alpha'_i(\lambda) = H(\lambda)\alpha_i(\lambda)$. The values of $I'(\lambda,t)$ are used to calculate the intensity at any wavelength and time, and thus the TRES. The values of the emission maxima and spectral width are determined by nonlinear least-square fitting of the spectral shape of the TRES. The spectral shape is assumed to follow a lognormal line shape [2],

$$I(\bar{\nu}) = I_0 \exp\left\{-\left[\ln 2\left(\frac{\ln(\alpha+1)}{b}\right)^2\right]\right\} \quad \ldots\ldots\ldots\ldots (5)$$

with $\alpha = \frac{2b(\bar{\nu} - \overline{\nu_{max}})}{b}$ >-1, where I_0 is amplitude, $\bar{\nu}_{max}$ is the wavenumber of the emission maximum and spectral width is given by, $\Gamma = \Delta\left[\frac{\sinh(b)}{b}\right]$

The terms b and Δ are asymmetry and width parameters. The equation (5) reduces to a Gaussian function for b=0. The solvation correlation function, C(t) is constructed following the equation, $C(t) = \frac{\nu(t) - \nu(\infty)}{\nu(0) - \nu(\infty)}$ where $\upsilon(0)$, $\upsilon(t)$ and $\upsilon(\infty)$ stand for the wavenumber in cm^{-1} at the emission maxima at time 0, t and infinity respectively. For anisotropy (r(t)) measurements, emission polarization is adjusted to be parallel or perpendicular to that of the excitation and anisotropy is defined as, $r(t) = \frac{[I_{para} - G \times I_{perp}]}{[I_{para} + 2 \times G \times I_{perp}]}$. G, the grating factor is determined following longtime tail matching technique [3] to be 1.2.

Results and Discussion:

To monitor the local dynamics of the protein and the nature of ligand binding in the different unfolded states, we have used three probes LDS 750, DCM and Coumarin 500.

Figure 1(a) shows the fluorescence transients at the blue and red end of the steady state emission spectrum at room temperature (25^0C) for the probe LDS 750 in protein solution. We have fitted the data upto 20 ns (solid line) and shown upto 2 ns to highlight the change in the decay pattern of the blue end from that in the red end of the emission spectrum. There is a fast decay in the blue end and rise in the red end of the emission spectrum indicating solvation stabilization of the probe in the protein environment. The constructed TRES (figure 1(b)) gives a spectral shift of 125 cm^{-1} in a 3 ns time window. The solvation correlation function (figure 2) decays with time constants of 0.147 ns (58%) and 0.687 ns (42%). The 0.147 ns component could be due to the solvation dynamics of bound water molecules inside the protein cavity [4] and the 0.687 ns component is associated with solvation due to the protein residues [5] and/or very rigid water molecules. The decay of the fluorescence anisotropy (inset of figure 2) gives a time constant of 50 ns associated with the global motion of the protein molecule [5, 6]. The fluorescence anisotropy decay shows that the probe resides in a rigid environment in the protein cavity with no appreciable rotational motion of its own. Figure 3(a) shows the temporal decay of the solvation correlation function associated with the probe LDS 750 in BSA at temperatures 50^0C and 75^0C. The time constants and the spectral shift associated with the decay of solvation correlation function of the probe-BSA complex at the two different temperatures have been tabulated in Table 1. At 50^0C the temporal decay of the solvation correlation function gives a time constant of 0.238 ns. The absence of the long component of $\approx$ 0.700 ns associated with the protein residue/rigid water solvation [5] as evidenced at 25^0C indicates that BSA swells up and accommodates more labile water molecules in its cavity. The spectral shift associated with the solvation shows

that we are losing a considerable portion of ultrafast solvation due to the labile water molecules in our instrumental resolution. The average time constants ($\tau_{av}=a_1\tau_1+a_2\tau_2$) associated with the decay of the solvation correlation functions for the probe decreases at 50^0C compared to that at 25^0C. At 75^0C the solvation correlation associated with the probe-protein complex decays with a time constant of 0.393 ns. This increase in time constant along with the increase in the associated spectral shift (Table 1) show that the probe in this unfolded state is solvated by protein residues which are now more labile to reorient along the excited dipole of the ligand LDS 750. Figures 3(b-c) shows the decay of fluorescence anisotropy associated with the probe LDS 750 at temperatures 50^0C and 75^0C respectively. The time constants (Table 2) associated with the fluorescence anisotropies are consistent with the bigger size of the unfolded protein at the two temperatures [6]. The percentage of this long component does not decrease even at 75^0C indicating that the probe is associated with the protein even in the unfolded state.

Figure 4(a) shows the decay of the solvation correlation function associated with the relaxation dynamics as experienced by the probe DCM bound to BSA at different temperatures. The time constants associated with the decay of the solvation correlation function (Table 1) of the DCM-BSA complex at 25^0C show that the DCM molecule enters into the hydrophobic region of its binding site in the protein. This binding site of the protein is only slightly affected when the temperature is raised to 50^0C. At 75^0C the environment around the DCM molecule shows a change in the time constants of the C(t) decays. The longer time constants associated with the temporal decay of the solvation correlation function at 75^0C suggest that there is increased solvation from the freely moving protein residues. The decrease in the spectral shift coupled with the red shift in

the emission maximum at time=0 indicates that a considerable part of the ultrafast hydration is lost in our instrumental resolution. The observation is consistent with the fact that the binding site opens up, exposing the protein residues and admitting water molecules inside the pocket. The decay of the fluorescence anisotropy associated with the DCM-BSA complex at different temperatures has been shown in figures 5(a-c). The time constants associated with the decays (Table 2) suggest that the DCM molecule does not leave the unfolded protein at 75^0C.

Figure 6(a) shows the solvation correlation functions of the probe Coumarin 500 in BSA at different temperatures. The time constants associated with the decay of the solvation correlation function has been listed in Table 1. The temporal decay of the solvation correlation function gives a time constant of 0.487 ns consistent with the solvation due to rigid water molecules and/or polar residues of the protein [5]. The emission of the probe in the protein complex at 25^0C shows a maximum at 490 nm. Comparison of the emission of the probe in hydrophobic (n-heptane, emission maximum=436 nm) and polar (water, emission maximum=500 nm) solvents at 25^0C suggests that the binding site of Coumarin 500 in the protein is probably a crevice in close contact with water molecules. In this regard the binding site of the probe is likely to be the binding site I located in sub-domain IIA of BSA molecule [7]. The emission maximum of the tryptophan residue located at the bottom of this binding site of structurally similar HSA shows a peak at 338 nm consistent with a more bulk like environment [7]. The time constants associated with the solvation correlation function at 50^0C suggest that the domain at which the probe resides changes considerably and due to opening of the crevice left the probe molecule is exposed to the bulk solvent giving time

constant of 0.077 ns (53%). The longer component of 3 ns (47%) associated with the solvation shows that the protein solvation is also a contributing factor. An increase in the spectral shift (Table 1) is also associated with the solvation at 50^0C. At 75^0C the binding site of the probe is completely destroyed [8] and the probe completely resides in a hydrophilic environment indicated by the time constant of 0.114 ns of the temporal decay of the solvation correlation function, C(t). The residence of the probe in the hydrophilic environment is also evidenced from the red shift in the steady-state emission peak and TRES peak at time=0. A decrease in the shift value associated with the solvation suggests that we are losing a considerable portion of ultrafast solvation in our resolution. The dynamics reported by the probe Coumarin 500 is consistent with the melting of domain II in the temperature range 50^0C-60^0C as reported in a previous study [8]. The temporal decays of the fluorescence anisotropies for the probe Coumarin 500 are shown in figure 7(a-c). The time constants associated with the decay are consistent with the thermal unfolding of the protein at 50^0C and 75^0C. The time constants associated with the decay of fluorescence anisotropy for the Coumarin 500-BSA complex at 75^0C, shows a 0.248 ns component in addition to the longer 70 ns component associated with the overall tumbling of the unfolded protein. This suggests that the probe Coumarin 500 is partially released into bulk buffer (since the average rotational time associated with the probe in bulk buffer is about 200 ps (data not shown)) after its binding site has been completely destroyed.

A comparison of the solvation characteristics along with the time constants associated with the temporal decay of fluorescence anisotropy of the three probes (Coumarin 500, DCM and LDS 750) clearly shows that the probes DCM and LDS 750 do

not bind to the same binding site as Coumarin 500. The analyses of the solvation correlation functions and the fluorescence anisotropies of the probe Coumarin 500 at different temperatures is consistent with the binding of the probe at sub domain IIA (site I) [8]. The similarity in the nature of variation of the solvation correlation function and the fluorescence anisotropies of the two probes DCM and LDS 750 at different temperatures suggest that the probes bind to the same site in the protein. On the other hand, the difference in the of variation of the solvation correlation function and the fluorescence anisotropies of the two probes DCM and LDS 750 at different temperatures with that of Coumarin 500 suggest that these two probes does not bind to site I. This leaves the likely possibility that the probes bind to the second site II (sub domain IIIA) in the protein.

References

[1] Lakowicz, J. R. (1999) Principles of fluorescence spectroscopy, Kluwer Academic/Plenum, New York.

[2] Horng, M. L., J. A. Gardecki, A. Papazyan and M. Maroncelli. (1995) Subpicosecond measurements of polar solvation dynamics: coumarin 153 revisited, *J. Phys. Chem.* **99**, 17311-17337.

[3] O'Connor, D. V. and D. Philips. (1984) Time correlated single photon counting, Academic Press, London.

[4] Kamal, J. K. A., L. Zhao and A. H. Zewail. (2004) Ultrafast hydration dynamics in protein unfolding: Human serum albumin, *Proc. Natl. Acad.Sci.USA* **101**, 13411-13416.

[5] Shaw, A. K., R. Sarkar, D. Banerjee, S. Hintschich, A. Monkman and S. K. Pal. (2007) Direct observation of protein residue solvation dynamics, *J. Photochem. Photobiol. A: Chem.* **185**, 76-85.

[6] Takeda, K. and K. Yamamoto (1989) Fluorescence lifetime and rotational correlation time of bovine serum albumin -sodium dodecyl sulphate complex labeled with 1-Dimethylaminonaphthalene -5- sulphonyl chloride: Effect of disulphide bridges in the protein on the fluorescence parameters, *Journal of Protein Chemistry* **9**, 17-22.

[7] Qiu, W., L. Zhang, Y. Y. Okobiah, L. Wang, D. Zhong and A. H. Zewail. (2006) Ultrafast solvation dynamics of human serum albumin : Correlations with conformational transitions and site selected recognition, *J. Phys Chem. B* **110**, 10540-10549.

[8] Flora, K., J. D. Brennan, G. A. Baker, M. A. Doody and F. V. Bright. (1998) Unfolding of acrylodan- labeled human serum albumin probed by steady state and time resolved fluorescence methods, *Biophysical Journal* **75**, 1084-1096.

Table 1: Solvation Correlation Function at different temperatures

	Temperature = 25^0C			Temperature = 50^0C			Temperature = 75^0C		
Probe	τ_1 (ns)	τ_2 (ns)	Shift (cm^{-1})	τ_1 (ns)	$\tau 2$ (ns)	Shift (cm^{-1})	τ_1 (ns)	τ_2 (ns)	Shift (cm^{-1})
LDS 750	0.147 (52%)	0.687 (48%)	125	0.238 (100%)	-	62	0.393 (100%)	-	109
Coumarin 500	0.489 (100%)	-	245	0.077 (53%)	0.987 (47%)	696	0.198 (100%)	-	157
DCM	0.235 (33%)	3.885 (67%)	560	0.236 (37%)	3.882 (63%)	825	0.790 (43%)	4.63 (57%)	350

Table 2: Fluorescence Anisotropy at different temperatures

	Temperature = 25^0C		Temperature = 50^0C		Temperature = 75^0C	
Probe	τ_1 (ns)	τ_2 (ns)	τ_1 (ns)	τ_2 (ns)	τ_1 (ns)	τ_2 (ns)
LDS 750		50 000 (100%)	0.841 (5%)	56.091 (95%)		74.010 (100%)
Coumarin 500	0.315 (8%)	50.000 (92%)	1.071 (12%)	51.901 (88%)	0.248 (30%)	70.223 (70%)
DCM	-	50.00 (100%)	1.651 (5%)	55.103 (95%)	-	70.102 (100%)

Figure Captions

Figure 1 (a) The fluorescence transients in the blue and red end of the probe LDS 750 in BSA at 25^0C. We have acquired 15 such transients to construct Time Resolved Emission Spectra (TRES). (b) The TRES of the probe LDS 750 in BSA at 25^0C.

Figure 2 The temporal decay of solvation correlation function, C(t) and fluorescence anisotropy, r(t) (inset) of the probe LDS 750 in BSA at 25^0C.

Figure 3 (a) The temporal decays of the solvation correlation function C(t) of the probe LDS 750 in BSA at 50^0C and 75^0C. The decay of fluorescence anisotropies, r(t) of the probe LDS 750 in BSA at 50^0C (b) and 75^0C (c).

Figure 4 The temporal decays of the solvation correlation function, C(t) of the probe DCM in BSA at different temperature.

Figure 5 The temporal decays of fluorescence anisotropies r(t) of the probe DCM in BSA at temperatures 25^0C (a), 50^0C (b) and 75^0C (c).

Figure 6 The temporal decays of the solvation correlation function C(t) of the probe Coumarin 500 in BSA at different temperature.

Figure 7 The temporal decays of fluorescence anisotropies r(t) of the probe Coumarin 500 in BSA at temperatures 25^0C (a), 50^0C (b) and 75^0C (c)

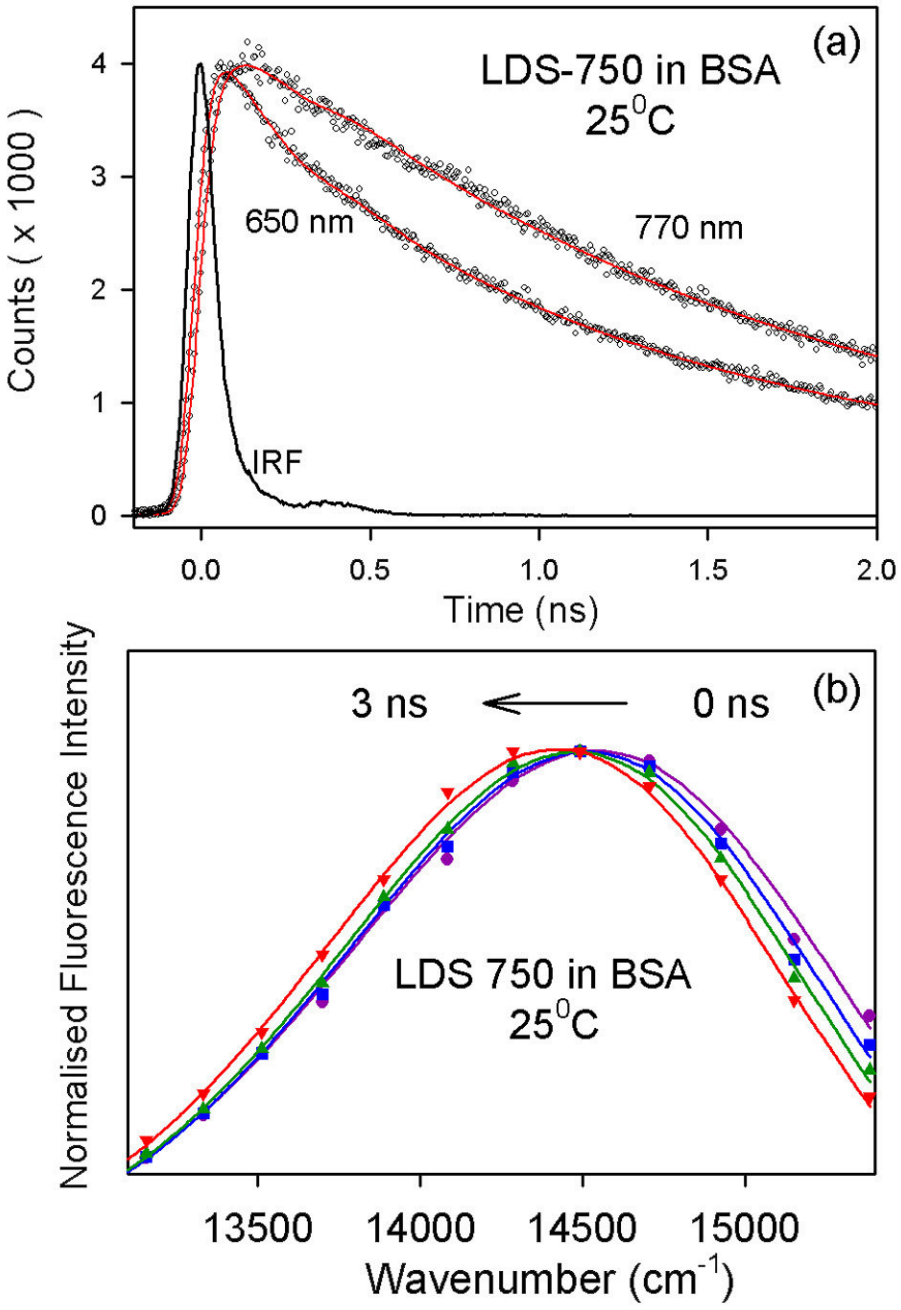
(a)
LDS-750 in BSA
25^{0}C
650 nm
770 nm
IRF
Counts (x 1000)
Time (ns)
(b)
3 ns
0 ns
LDS 750 in BSA
25^{0}C
Normalised Fluorescence Intensity
Wavenumber (cm^{-1})

Figure 1

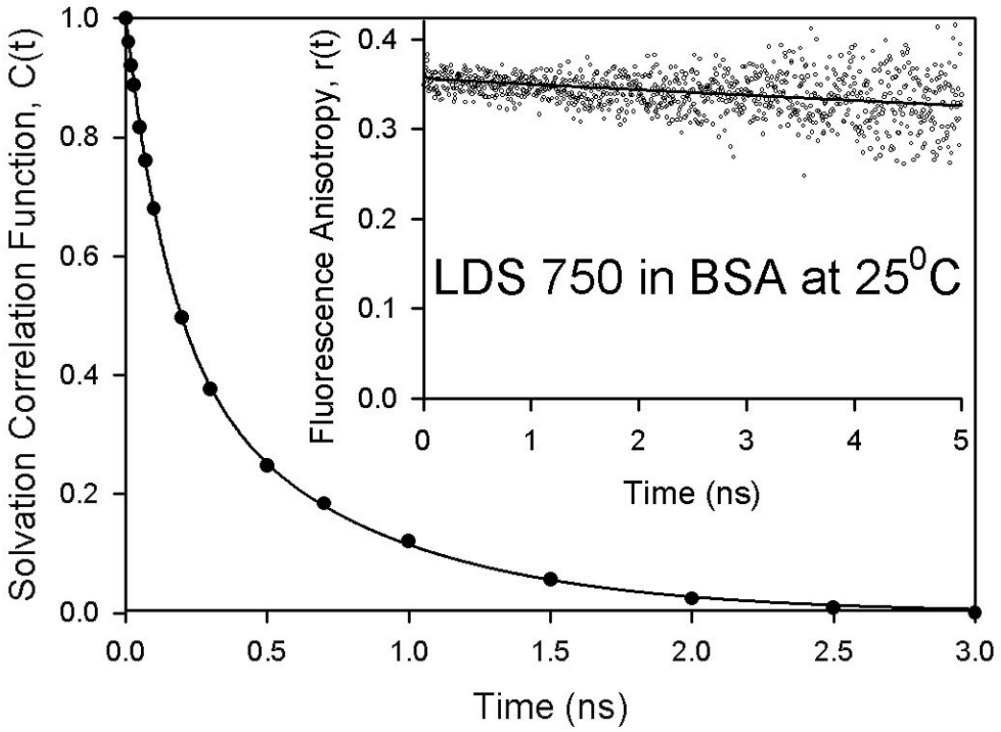
Solvation Correlation Function, C(t)
Time (ns)
Fluorescence Anisotropy, r(t)
Time (ns)
LDS 750 in BSA at 25^{0}C

Figure 2

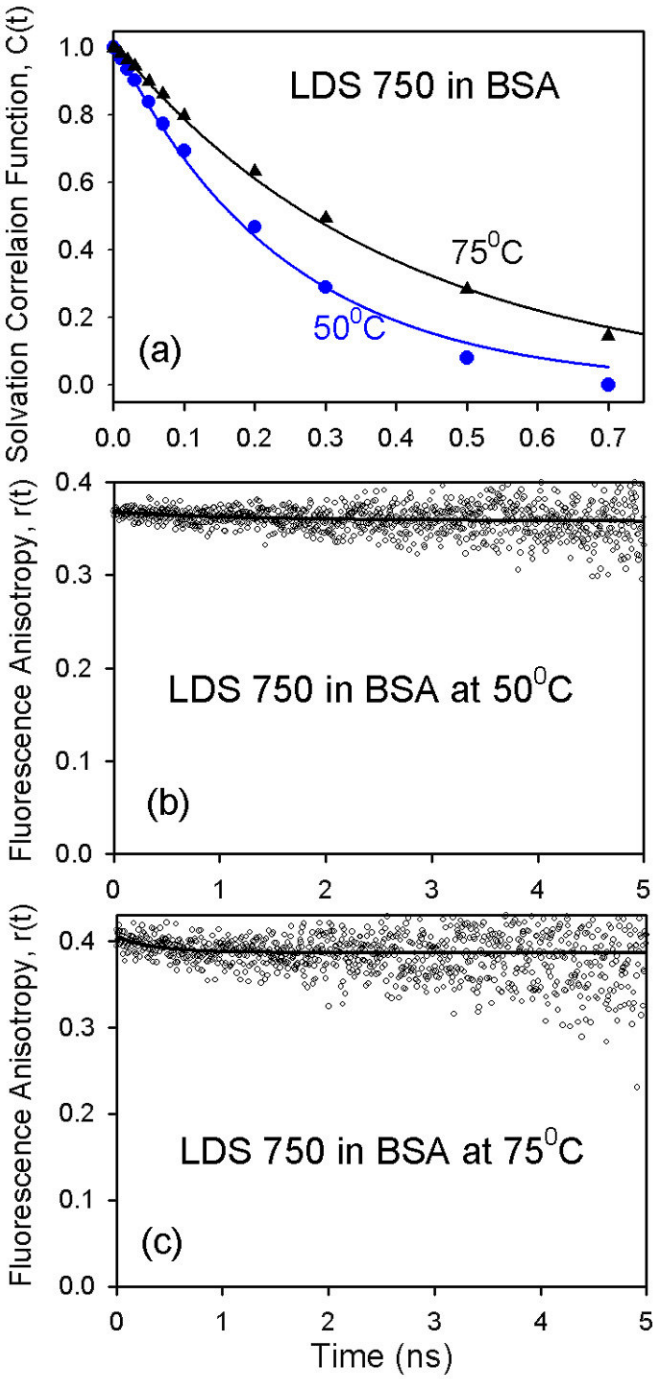
Solvation Correlaion Function, C(t)
LDS 750 in BSA
75^{0}C
50^{0}C
(a)
Fluorescence Anisotropy, r(t)
LDS 750 in BSA at 50^{0}C
(b)
Fluorescence Anisotropy, r(t)
LDS 750 in BSA at 75^{0}C
(c)
Time (ns)

Figure 3

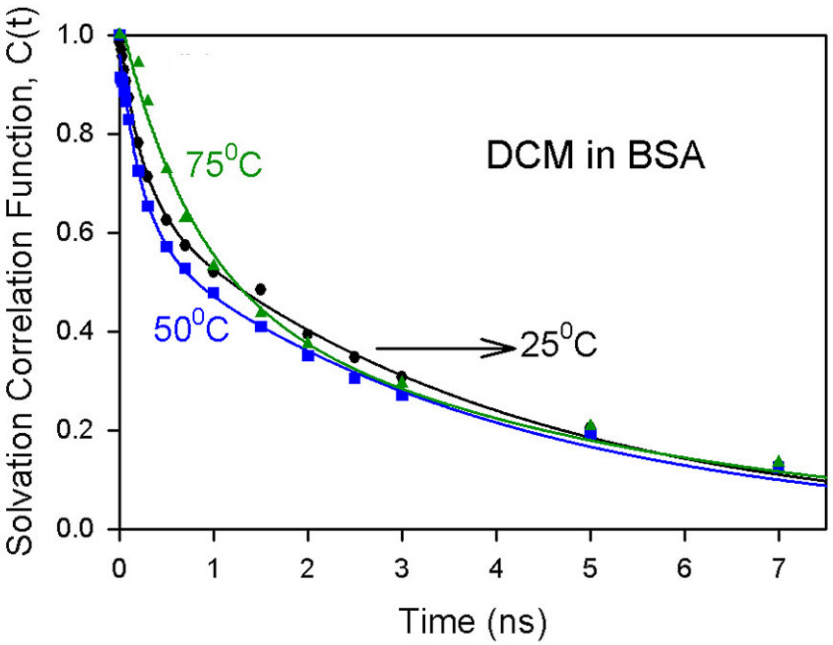
Solvation Correlation Function, C(t)
1.0
0.8
0.6
0.4
0.2
0.0
0
1
2
3
4
5
6
7
Time (ns)
75^{0}C
50^{0}C
25^{0}C
DCM in BSA

Figure 4

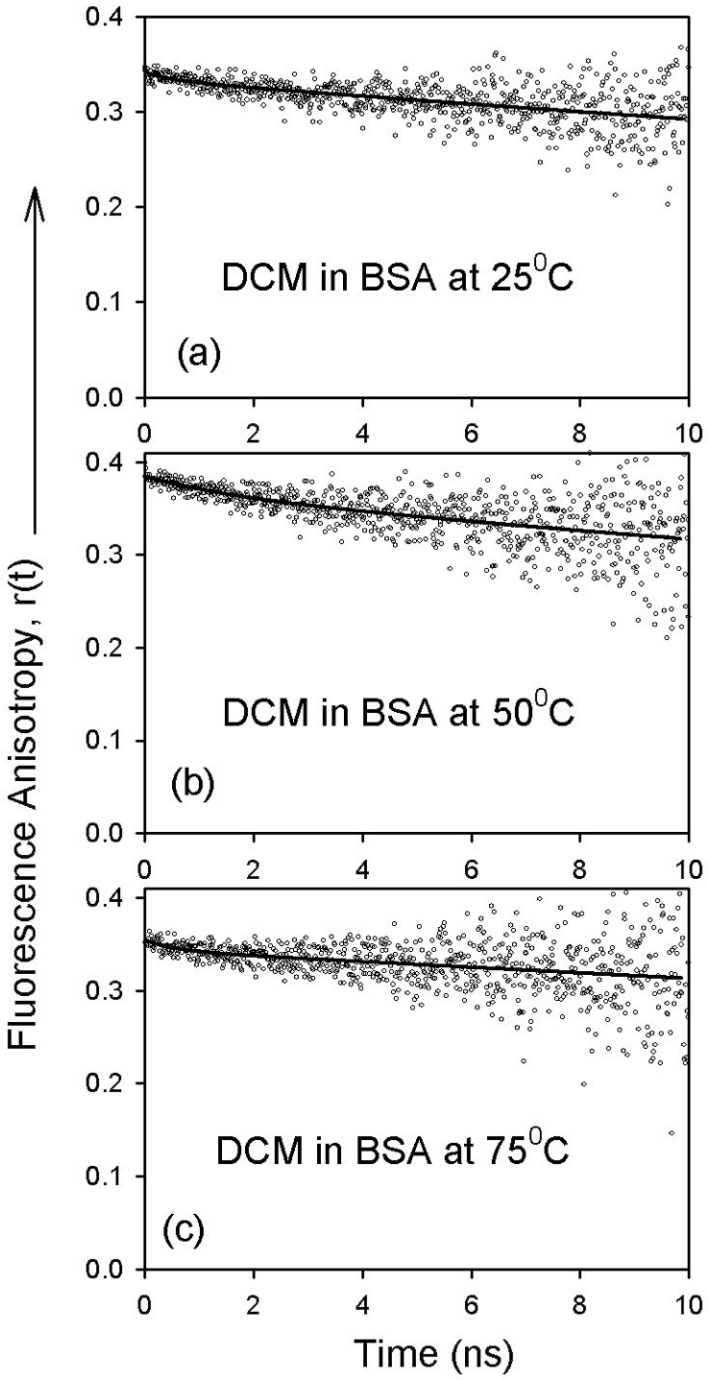
Fluorescence Anisotropy, r(t)
DCM in BSA at 25^{0}C
(a)
DCM in BSA at 50^{0}C
(b)
DCM in BSA at 75^{0}C
(c)
Time (ns)
0.0
0.1
0.2
0.3
0.4
0
2
4
6
8
10

Figure 5

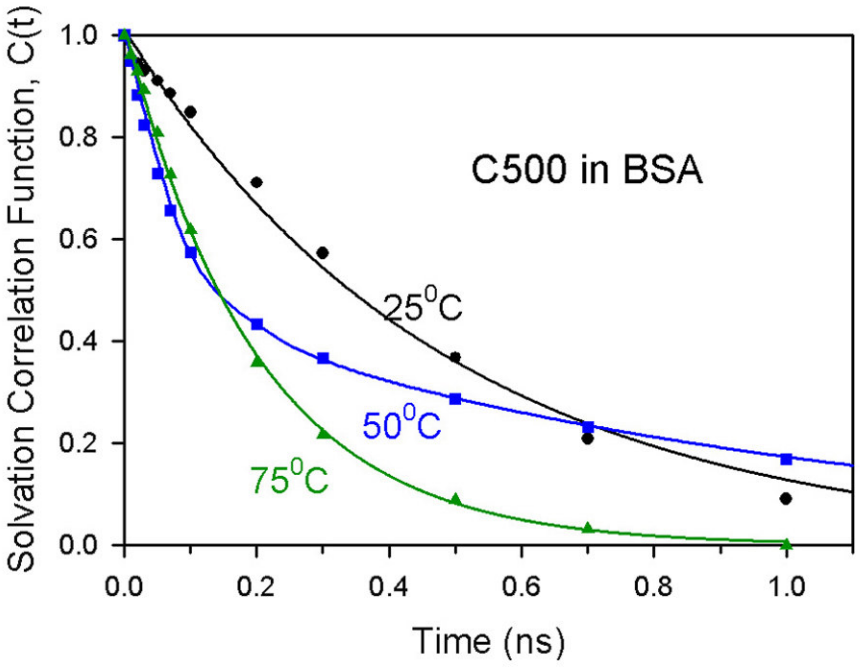
Solvation Correlation Function, C(t)
1.0
0.8
0.6
0.4
0.2
0.0
0.0
0.2
0.4
0.6
0.8
1.0
Time (ns)
C500 in BSA
25^{0}C
50^{0}C
75^{0}C

Figure 6

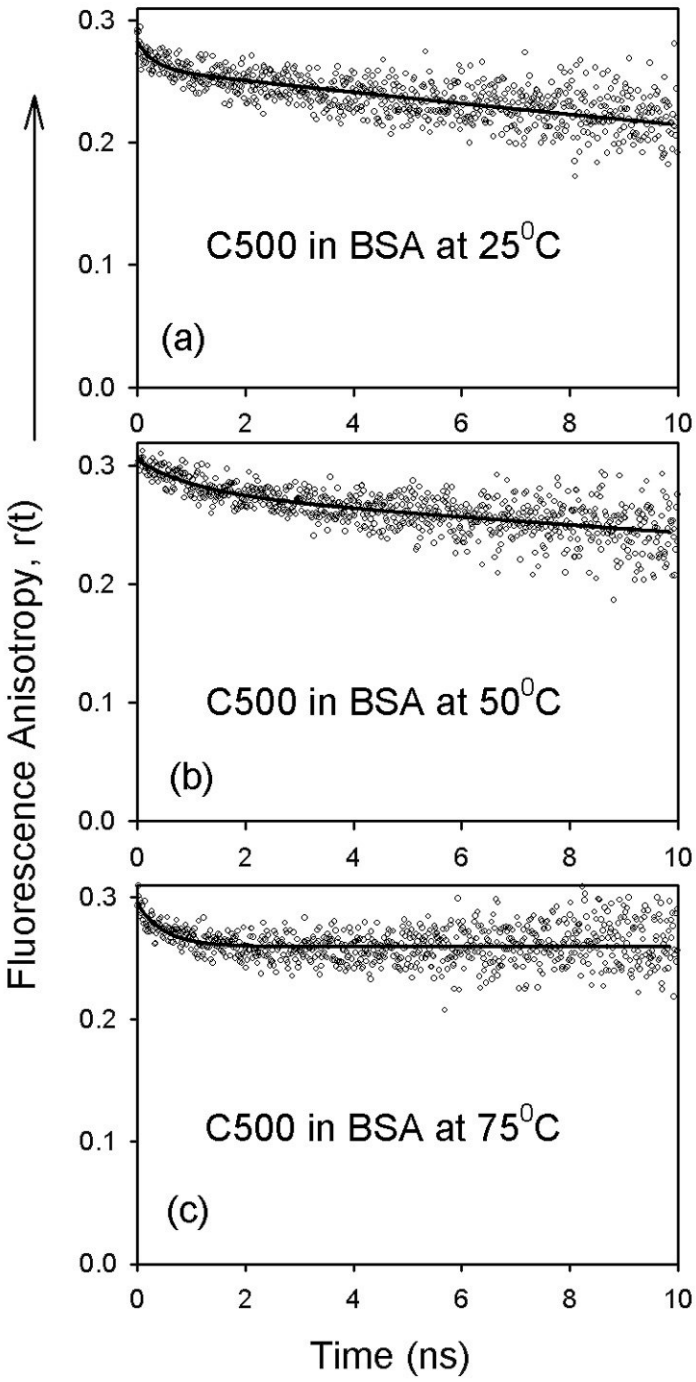
Fluorescence Anisotropy, r(t)
C500 in BSA at 25^{0}C
(a)
C500 in BSA at 50^{0}C
(b)
C500 in BSA at 75^{0}C
(c)
0.0
0.1
0.2
0.3
0
2
4
6
8
10
Time (ns)

Figure 7